

# Adsorption and dissociation of H<sub>2</sub>O monomer on ceria(111): Density functional theory calculations

Shuang-Xi Wang,<sup>1,2,3</sup> Ping Zhang,<sup>3,\*</sup> and Shu-Shen Li<sup>1</sup>

<sup>1</sup>*State Key Laboratory for Superlattices and Microstructures, Institute of Semiconductors, Chinese Academy of Sciences, P. O. Box 912, Beijing 100083, People's Republic of China*

<sup>2</sup>*Department of Physics, Tsinghua University, Beijing 100084, People's Republic of China*

<sup>3</sup>*LCP, Institute of Applied Physics and Computational Mathematics, P.O. Box 8009, Beijing 100088, People's Republic of China*

The adsorption properties of isolated H<sub>2</sub>O molecule on stoichiometric and reduced ceria(111) surfaces are theoretically investigated by first-principles calculations and molecular dynamics simulations. We find that the most stable adsorption configurations form two hydrogen bonds between the adsorbate and substrate. The water molecule is very inert on the stoichiometric surface unless up to a high temperature of 600 K. For the reduced surface, we find that the oxygen vacancy enhances the interaction. Moreover, simulations at low temperature 100 K confirm that it is facilitated for water to dissociate into H and OH species.

PACS numbers: 68.43.Bc, 68.43.Fg, 68.43.Jk, 68.47.Gh

## I. INTRODUCTION

Ceria (CeO<sub>2</sub>) is a crucial material for catalytic applications due to its remarkable properties<sup>1,2</sup>. One of its important application is that ceria can effectively promote the water-gas shift reaction,  $\text{CO} + \text{H}_2\text{O} \rightarrow \text{CO}_2 + \text{H}_2$ , by which converting harmful carbon monoxide to the less harmful carbon dioxide, and generating hydrogen. A full account of the involved mechanism has not been achieved, while the interactions between water and ceria surface may play a key role during the reaction.

Therefore, a systematic study of the fundamental interactions involved in the water-ceria system is much desirable. The oxygen-terminated ceria(111) surface, which is most often found in experiments<sup>3</sup>, has been identified to be energetically the most stable<sup>4-7</sup>. The formation of oxygen vacancies in ceria, hence reducing the cerium from Ce<sup>4+</sup> to Ce<sup>3+</sup>, is closely related to its interesting properties and important implications, such as oxygen storage capacity of ceria<sup>1</sup>. A heavily debated question is on the favorable position of the oxygen vacancy. Theoretically, different research methods including density-functional theory (DFT) calculations, have given different favorable vacancy sites (on-surface or on-subsurface)<sup>8,9</sup>. For the interaction between adsorbate and ceria surface, obviously, the on-surface oxygen vacancy is much concerned.

Experimentally, it has been found that water on reduced ceria powders can effectively oxidize Ce<sup>3+</sup> into Ce<sup>4+</sup>, with the H<sub>2</sub> production<sup>10-12</sup>. More recently, evidences have been provided by Henderson *et al.*<sup>13</sup> for that the water may split at low temperature below 170 K, and exposure of water at 650 K results in additional surface reduction of ceria instead of oxidation. In addition, they offered three potential adsorption geometries for water on the stoichiometric ceria(111) surface, namely, the so-called C<sub>2v</sub> geometry without hydrogen bond between the water and the substrate (no-H-bond), single hydro-

gen bond (one-H-bond), and two hydrogen bonds (two-H-bond) configurations, needing to be examined by theoretical calculations.

Several theoretical works have investigated the H<sub>2</sub>O-ceria interaction by DFT calculations. Kumar *et al.*<sup>14</sup> reported that the water adsorption on the stoichiometric ceria(111) surface favors one-H-bond configuration, consistent with the later literature results<sup>15,16</sup>. While this conflicts with the results obtained by Fronzi *et al.*<sup>17</sup>, who suggested a two-H-bond structure. For water on reduced (with on-surface oxygen vacancy) ceria(111) surface, the calculated stable adsorption structures varied from no-H-bond<sup>16,17</sup>, to one-H-bond<sup>14</sup> configuration, while Chen *et al.*<sup>15</sup> found no binding between water and reduced surface. Moreover, Kumar *et al.*<sup>14</sup> predicted that oxidation of the reduced surface by water with the production of hydrogen gas is weakly exothermic, while Yang *et al.*<sup>16</sup> and Fronzi *et al.*<sup>17</sup> argued that hydroxyl surface forms upon water dissociating.

Such discrepancies may partially arise from the different unit cell adopted by different authors. Actually, the water coverage adopted in previous works ranges 0.25–1.0 ML. Too high water coverage would be problematic because it may mask the true H<sub>2</sub>O-ceria interaction, by the dipole-dipole interactions between adjacent water molecules. Therefore, a systematical study of water on stoichiometric and reduced ceria(111) surfaces at lower coverage, which minimizes the lateral interaction between the adsorbates, is indispensable to shed a light on such discrepancies for a proper understanding of water adsorption on ceria(111) surface.

The DFT+*U* calculations based on first-principles method have proved to be an effective approach for studying the strong correlation materials consisting *d* and *f* electrons, compared with the plain DFT method<sup>18</sup>. For bulk ceria, there has been a vast literature dealing with this issue, despite the controversial determination of the Hubbard parameter *U*<sup>6,14,19-21</sup>. For the

surface properties of ceria, however, by declaring its negligible influence, little work takes into consideration the  $U$  parameter<sup>4-7</sup>. Nevertheless, it has been revealed that the plain DFT method failed to correctly describe the behavior of the water molecule on reduced ceria surface<sup>16,17</sup>. Due to the localization of  $f$  electrons, especially for reduced ceria surfaces with oxygen vacancies, to describe more accurately the excess electrons, strong correlation effect must be considered<sup>14,19</sup>, hence the DFT+ $U$  approach is required. In addition to the static DFT calculation, *ab initio* molecular dynamics (AIMD) simulations can effectively demonstrate the dynamical properties of a system when considering temperature, which can be compared with the existing experimental measurements. Moreover, the use of AIMD can be a beneficial complement to the static calculations, especially for systems showing multiple low-lying minima in energy<sup>22</sup>.

In the present work, we systematically study the properties of isolated water adsorption on stoichiometric and reduced ceria(111) surfaces at low coverage by means of first-principles methods. We perform the microscopic static DFT calculations aiming at elucidating the electronic structure and static stability for the water adsorption structures. Besides, AIMD simulations at various temperatures are also conducted to investigate the dynamical properties of these systems.

## II. COMPUTATIONAL METHOD

The calculations are performed within DFT using the projector-augmented wave (PAW) method, as implemented in the plane-Wave based Vienna *ab-initio* simulation package (VASP)<sup>23</sup>. The cutoff energy for the plane wave expansion is set to 400 eV. For the bulk ceria, the exchange and correlation effects are treated within both the local density approximation (LDA) and the PBE<sup>24</sup> generalized gradient approximation (GGA). For the ceria surface, however, only LDA is adopted. Here the cerium  $5s$ ,  $5p$ ,  $5d$ ,  $4f$ , and  $6s$ , and the oxygen  $2s$  and  $2p$  electrons are treated as valence electrons. We use the DFT+ $U$  formalism formulated by Dudarev *et al.*<sup>25</sup> to account for the strong on-site Coulomb repulsion amongst the localized Ce  $4f$  electrons. In this scheme the on-site two-electron integrals, expressed in terms of two parameters, i.e., the Hubbard parameter  $U$ , which reflects the strength of the on-site Coulomb interaction, and the parameter  $J$ , which adjusts the strength of the exchange interaction, are combined into a single parameter  $U_{\text{eff}} = U - J$ , indicating that only the difference between  $U$  and  $J$  is significant. For the bulk ceria, the Coulomb  $U$  is treated as a variable, while the exchange energy  $J$  is set to be 0.7 eV. Then the parameter  $U_{\text{eff}}$  is fixed at a reasonable specific value for the surface calculations.

The oxygen-terminated ceria(111) surface is modeled by a slab composing of six atomic layers and a vacuum region of 15 Å. A  $(3 \times 3)$  surface unit cell, in which each monolayer contains nine atoms, is adopted in the study

of the H<sub>2</sub>O adsorption. The isolated H<sub>2</sub>O molecule is placed on one side of the slab, equivalent to 1/9 coverage. Our test calculations have showed that such low a coverage is sufficient to avoid the interaction between adjacent H<sub>2</sub>O molecules, hence makes the true H<sub>2</sub>O-ceria interaction emerge. During our calculations, the bottom two atomic layers of the substrate are fixed, and other atoms as well as the H<sub>2</sub>O molecule are free to relax until the forces on the ions are less than 0.03 eV/Å. Integration over the Brillouin zone is done using the Monkhorst-Pack scheme<sup>26</sup>. For bulk ceria, we use a  $9 \times 9 \times 9$  grid points, and for the surface we use a  $3 \times 3 \times 1$  grid points.

The calculations of the energy barriers for the water diffusion and dissociation processes are performed using the climbing image nudged elastic band (CI-NEB) method<sup>27</sup>, which is an improved version of the traditional NEB method<sup>28</sup> for finding minimum energy reaction paths between two known minimum energy sites, resulting in a more accurate estimation of the activation energy than the regular NEB method does, by driving up one of the intermediate states near the transition point to reach the highest saddle point along the reaction path.

For AIMD calculations, the Born-Oppenheimer approximation is used; ions are considered as classical objects moving on the potential surface created by the electrons obeying the quantum mechanical equation. The canonical ensemble using the Nosé thermostat<sup>29</sup> is employed. Electronic energies are converged up to  $10^{-6}$  eV. With a time step of 1 fs, initial equilibration steps are performed over 1 ps, while production runs are 6 ps long.

## III. RESULTS AND DISCUSSION

### A. Determination of bulk properties of ceria

The stoichiometric ceria crystallizes in a CaF<sub>2</sub>-like ionic structure with space group  $Fm\bar{3}m$ . The experimentally determined lattice parameter is about 5.41 Å<sup>30,31</sup>, and the bulk modulus varies over a rather broad range of 204 to 236 GPa<sup>30-33</sup>. In this section we demonstrate the dependence of the lattice parameter  $a_0$  and bulk modulus  $B$  on  $U_{\text{eff}}$  in the range  $0 \sim 8$  eV, obtained by fitting the third-order Birch-Murnaghan equation of state<sup>34</sup>, as presented in Fig. 1.

We can see from Fig. 1 that the reasonable lattice parameter values  $a_0$  are 5.40 Å (LDA+ $U$ ,  $U_{\text{eff}}=5$  eV) and 5.48 Å (GGA+ $U$ ,  $U_{\text{eff}}=3$  eV), and the bulk modulus values  $B$  are 210.3 GPa (LDA+ $U$ ) and 178.4 GPa (GGA+ $U$ ). Noticeably, our calculations are consistent with previous studies of Andersson *et al.*<sup>20</sup> and Loschen *et al.*<sup>21</sup>, but we can not reproduce the results obtained by Jiang *et al.*<sup>6</sup>. It is clear that the GGA+ $U$  calculations overestimate the lattice parameter and underestimated the bulk modulus, and thus give a slightly less accurate description of the atomic structure of ceria. On the other hand, LDA+ $U$  proposes a reasonable description. Moreover, within the latter choice, the calculated O2p-Ce4f

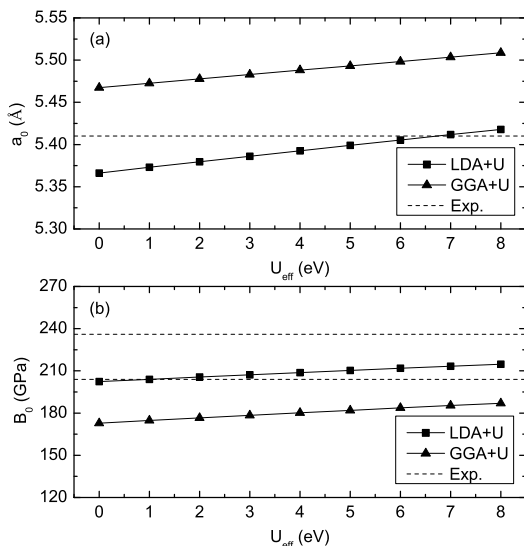


FIG. 1: Dependence of the lattice parameter (a) and bulk modulus (b) of  $\text{CeO}_2$  on  $U_{\text{eff}}$ . The dotted lines stand for the experimental measurements.

and  $\text{O}2p\text{-Ce}5d$  band gaps are 2.21 and 5.29 eV, consistent with the experimental measurements of about 3 and 6 eV, respectively<sup>35</sup>. Moreover, it has been revealed that the LDA treatment is actually better than the GGA ones when simulating chemical reactions on reduced ceria surfaces<sup>19</sup>. In addition, as mentioned above, most of the previous DFT calculations dealt with the  $\text{H}_2\text{O}$ -ceria interactions by using GGA functional<sup>14-17</sup>, with somewhat conflicting results existing, hence the LDA treatment can be performed as a beneficial complement. Therefore, in the following surface calculations, we will present only the LDA+ $U$  results.

### B. $\text{H}_2\text{O}$ adsorption on stoichiometric ceria(111)

The structural and energetic parameters of the free water molecule are calculated within a box with the same size of the adsorbed systems. The optimized geometry for free  $\text{H}_2\text{O}$  gives a bond length of 0.97 Å and a bond angle of  $105.2^\circ$ , consistent with the experimental values of 0.96 Å and  $104.4^\circ$ <sup>36</sup>.

The adsorption energy of the system is calculated as follows:

$$E_{\text{ad}} = E_{\text{H}_2\text{O}/\text{ceria}(111)} - E_{\text{H}_2\text{O}} - E_{\text{ceria}(111)}, \quad (1)$$

where  $E_{\text{H}_2\text{O}}$ ,  $E_{\text{ceria}(111)}$ , and  $E_{\text{H}_2\text{O}/\text{ceria}(111)}$  are the total energies of the  $\text{H}_2\text{O}$  molecule, the clean ceria(111) surface, and the adsorption system respectively. According to this definition, a negative value of  $E_{\text{ad}}$  indicates that the adsorption is exothermic (stable) with respect to a free  $\text{H}_2\text{O}$  molecule and a positive value indicates endothermic (unstable) reaction.

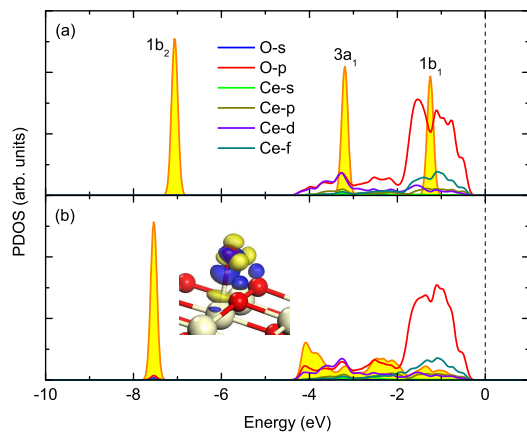


FIG. 2: (Color online) PDOS for the  $\text{H}_2\text{O}$  molecule and the first-layer O and the second-layer Ce of the stoichiometric surface for (a) free  $\text{H}_2\text{O}$  and the clean ceria(111) surface, (b) the A1 adsorption site. The inset in (b) shows the 3D electron density difference, with the isosurface value set at  $\pm 0.05 \text{ e}/\text{\AA}^3$ . The area filled with yellow color represents MOs of  $\text{H}_2\text{O}$ . The Fermi level is set to zero.

Adsorption geometry optimizations are performed for a variety of initial orientations of the  $\text{H}_2\text{O}$  molecule placed over different surface sites, i.e., the flat-lying (water molecule lying parallel to the surface), O-down (O atom pointing to the surface) and H-down (two H atoms pointing to the surface) structures. We identify different  $\text{H}_2\text{O}$  adsorption structures, whereas only the low-energy one (A1) is discussed here, with the adsorption energy of  $-0.96 \text{ eV}$  and the corresponding frequencies of 3269.7, 3206.8, and  $1490.3 \text{ cm}^{-1}$ . The equilibrium geometry of A1 state is illustrated in the inset of Fig. 2, in which the adsorbed  $\text{H}_2\text{O}$  monomer lies nearly parallel to the surface, with the O atom of water located almost on top of the second-layer Ce atom, while H atoms symmetrically oriented pointing to the first-layer O atoms ( $d_{\text{O-H}}=1.85 \text{ \AA}$ ), namely, with two-H-bond configuration formed, in agreement with the results of Fronzi *et al.*<sup>17</sup>. Noteworthy, this adsorption configuration is quite different from previous studies, either the arbitrary assumption of the no-H-bond<sup>13</sup> or the one-H-bond<sup>14-16</sup> configuration. The difference may arise from that those previous studies underestimated the hydrogen bond strength, which plays a key role in the interactions between water and oxide surfaces. Moreover, the dipole-dipole interactions between adsorbed water molecules at high coverage probably blur the exact monomer adsorption configuration studied in this letter.

In order to further understand the precise nature of the chemisorbed molecular state, we plot in Fig. 2 the electronic projected density of states (PDOS) of the molecular adsorption structure for the stable adsorption configuration of A1 in comparison with those of free  $\text{H}_2\text{O}$  molecule and clean ceria(111) surface. The three-dimensional (3D) electron density difference  $\Delta\rho(\mathbf{r})$ ,

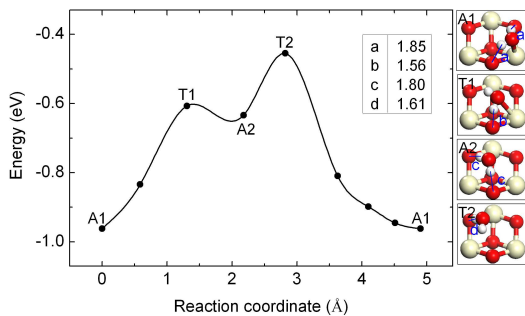


FIG. 3: (Color online) Variation in  $\text{H}_2\text{O}$  adsorption energy on the stoichiometric ceria(111) surface as a function of the lateral displacements of O atom from its original adsorption site A1 to the nearest-neighbor one. Insets show the corresponding geometry sketches for minima (A1, A2) and transition (T1, T2) states. The chart summarizes the targeted O-H distances (in Å) pointed out in the insets. Large, moderate and small spheres stand for Ce, O and H atoms, respectively.

which is obtained by subtracting the electron densities of noninteracting component systems,  $\rho^{\text{ceria}(111)}(\mathbf{r}) + \rho^{\text{H}_2\text{O}}(\mathbf{r})$ , from the density  $\rho(\mathbf{r})$  of the  $\text{H}_2\text{O}/\text{ceria}(111)$  system, while retaining the atomic positions of the component systems at the same location as in  $\text{H}_2\text{O}/\text{ceria}(111)$ , is also shown in the inset of Fig. 2 (b). Positive (blue)  $\Delta\rho(\mathbf{r})$  indicates accumulation of electron density upon binding, while a negative (yellow) one corresponds to electron density depletion. Molecular orbital (MO)  $2a_1$  of water (not shown here) is far below the Fermi level and thus remains intact in water-metal interaction. Here we consider only three MOs  $1b_2$ ,  $3a_1$ , and  $1b_1$ .

As illustrated in Fig. 2, upon adsorption, the orbital  $1b_2$  is observed to shift down in energy by 0.47 eV. More significantly, the orbitals  $3a_1$  and  $1b_1$  undergo noticeable changes, especially for the latter, becoming more broadened and hence apparently delocalized, with the domain of energy corresponding to that of the ceria surface. Obviously, the  $d$ - and  $f$ -states of the Ce atom do not change much because of localization. On the other hand, the shifting up in energy for the peak of O- $2p$  states of the ceria surface play a key role in the water-ceria interaction, which indicates that the adsorbed MO  $1b_1$  may act as an electron donor state. The features of the orbital hybridization are further substantiated by the 3D electron density difference plotted in the inset of Fig. 2(b). We can see that there exists a large charge accumulation beneath the O atom of the adsorbate. This accumulation should come from the charge redistribution because of delocalization of the MOs of water, rather than from the substrate, which is consistent with above PDOS analysis demonstrating the localization of Ce electronic states. Moreover, obvious charge transfer from H atoms of the adsorbate to the surface O atoms is observed, suggesting strong hydrogen-bond interactions between the adsorbate and substrate.

Given a  $\text{H}_2\text{O}$  molecule at a stable adsorption site, it is

interesting to see how it diffuses on the substrate. Therefore, we calculate the diffusion path and energetic barrier of water on ceria(111) surface between neighboring stable A1 sites, with the adsorption energy as a function of the lateral displacement of O atom of the water molecule shown in Fig. 3. As indicated, the molecular A1 state is adsorbed by  $-0.96$  eV. Along the diffusion path, the system evolves through an energy barrier of 0.35 eV to reach a semi-stable state A2, which is also nearly flat on the surface. A2 is less stable with an adsorption energy of  $-0.63$  eV, with the O atom of water located on top of the third-layer O atom, while as in the A1 state, two hydrogen bonds formed between H atoms of the water and the surface-layer O atoms ( $d_{\text{O-H}}=1.80$  Å). At the transition state T1, one H atom of the water points to the top O atom, with the distance  $d_{\text{O-H}}=1.56$  Å. Along this path, the diffusion from A2 to the neighboring A1 is hindered by a barrier of 0.18 eV, across the transition state T2, which also forms single hydrogen bond. It can be seen from the transition states T1 and T2 that the single hydrogen bond formed between the water monomer and the oxide surface is unfavored in energy, which is different from the previous high-coverage studies<sup>14</sup> but consistent with our finding that the two-hydrogen-bond interaction is favored for the monomer adsorption.

According to the overall energetic profile obtained above, we calculate the diffusion coefficient at different values of temperature  $T$  of this system within the Arrhenius-type relation,  $D = \nu_0 d^2 e^{-\varepsilon/k_B T}$ , where  $\nu_0=3269.7$   $\text{cm}^{-1}$  is the vibrational frequency of A1 state,  $d=4.90$  Å is the displacement of the water during diffusion, and  $\varepsilon=0.51$  eV is the activation energy. For comparison the diffusion coefficient at  $T=300$  K and 600 K are calculated to be  $7.18 \times 10^{-14}$  and  $1.30 \times 10^{-9}$   $\text{m}^2/\text{s}$ , respectively. It is clear that at 300 K, the coefficient is too small to facilitate the diffusion process. While at 600 K, diffusion should be observed easily.

This is confirmed by our AIMD simulations, starting from the adsorbed molecular site A1 at 300 K and 600 K, which are shown in Fig. 4. At room temperature (300 K), it can be seen that the molecular state A1 is recovered with only small oscillations. Apparently the H atom oscillates more intensely than the O atom, with the longest  $d_{\text{O-H}}=1.54$  Å in the water molecule. At higher temperature of 600 K, the water molecule undergoes more considerable oscillations (with the longest  $d_{\text{O-H}}=1.63$  Å), and finally negotiates a diffusion to the neighboring adsorption site A1, as identified in the above CI-NEB calculations.

Moreover, during AIMD simulations we find that at temperature as high as 600 K, neither desorbed nor dissociated water configuration is observed. This indicates that on one hand the water-oxide interaction is strong enough to stand for high temperature, on the other hand, the stoichiometric ceria surface is inactive towards  $\text{H}_2\text{O}$  splitting. Actually, by static calculations, we find that the co-adsorption of H and OH species on the regular ceria(111) surface is endothermic thus unstable. In a word,

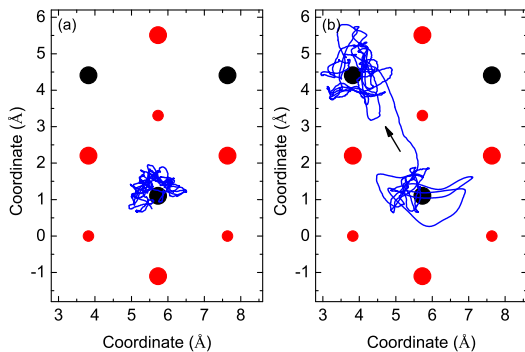


FIG. 4: (Color online) Projection on the stoichiometric ceria(111) surface of the position of the oxygen atom (blue) corresponding to the H<sub>2</sub>O from AIMD simulation at the temperature of 300 K (a) and 600 K (b), respectively. The black arrowhead in (b) denotes the diffusion orientation. The large red and black filled circles mark the equilibrium positions of the first-layer O atoms and the second-layer Ce atoms, respectively, while the smaller red ones represent the third-layer O atoms.

the stoichiometric ceria(111) surface does not dissociate water, in good agreement with previous calculations<sup>14–17</sup>. However, the existence of defects, especially the oxygen vacancies on the surface of ceria, may act as active sites for the dissociation of water. Hence, in the following section we will focus our attention on this topic.

### C. H<sub>2</sub>O adsorption on reduced ceria(111)

It has been proposed that for bulk ceria, the oxygen-vacancy formation process is facilitated by a simultaneous condensation of two electrons into localized *f*-level traps on two cerium atoms<sup>37</sup>. The situation is similar for ceria surface<sup>5</sup>. We can see from Fig. 5(a) that in the reduced surface the Ce-*4f* states become partially occupied, meanwhile other states of the surface remain almost intact, compared with that in stoichiometric surface. This observation may contribute much to the adsorption properties of water on the reduced ceria surface.

Similarly to the stoichiometric surface, we explore different H<sub>2</sub>O adsorption structures and find that the most stable molecular adsorption state is A2 adjacent to the defect (labeled A2') with the adsorption energy of  $-1.09$  eV, while A1 adjacent to the defect is the next most stable state (labeled A1') with the adsorption energy of  $-0.93$  eV. As illustrated in the insets of Fig. 6, for these two stable molecular states, the distances between the H atoms of water and first-layer O atoms are 1.77 and 1.82 Å, respectively, both smaller than that on the stoichiometric surface. In A2' configuration the O atom of the adsorbed water is located on top of the third-layer O atom, with a lower adsorption energy compared with that on the stoichiometric surface. Apparently, as depicted by previous studies<sup>14–17</sup>, the oxygen vacancy enhances the

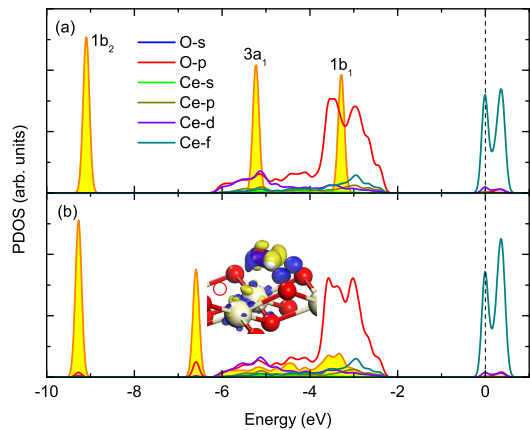


FIG. 5: (Color online) PDOS for (a) free H<sub>2</sub>O and the clean reduced ceria(111) surface, (b) the A2' adsorption site. The isosurface value for the 3D electron density difference is set at  $\pm 0.05 e/\text{\AA}^3$ . The red open circle in the inset of (b) denotes the oxygen vacancy position. The Fermi level is set to zero.

water-ceria interaction.

Figure 5(b) presents the PDOS of the molecular state A2'. One can see that the MOs  $1b_2$  and  $3a_1$  keep localized, only with a down-shift in energy by 0.16 and 1.36 eV, respectively, while  $1b_1$  becomes totally delocalized, which gives the main contribution to the adsorption behavior of water monomer. In addition, the other contribution to the adsorption behavior comes from the O- $2p$  states of the surface, and the water adsorption introduces new peak for  $2p$  states of the surface O atom, aligning in energy with  $3a_1$ . From the 3D electron density difference, we can observe more obvious charge transfer from H atoms of the water to the surface O atoms, compared with that on stoichiometric surface, probably providing a reason why the water molecule adsorbs to the reduced surface more strongly. Resembling that on the stoichiometric surface, the partially filled Ce  $4f$  state almost does not participate the interaction with water, which exactly reveals the importance of the Hubbard parameter  $U$  for correctly depicting its localization. Moreover, we notice that this parameter prominently dominates the bulk properties of ceria such as lattice constant, hence indirectly holds the interactions between water and substrate, particularly for the reduced ceria(111) surface.

To clarify how an oxygen vacancy affects the dynamical properties of the adsorbed water monomer, let us examine the diffusion and dissociation of the H<sub>2</sub>O molecule on this reduced surface. We calculate the diffusion path of the water between the stable states A2' and A1' (see Fig. 6). It is clear that the diffusion from A2' to A1' needs to overcome an energy barrier of 0.44 eV, while the inverted diffusion from A1' to A2' is more facilitated with a lower barrier of 0.27 eV. Noticeably, the diffusion energy barriers presented here are larger than that on the stoichiometric ceria surface, and this should be attributed to the rotation of H<sub>2</sub>O molecule during the diffusion pro-

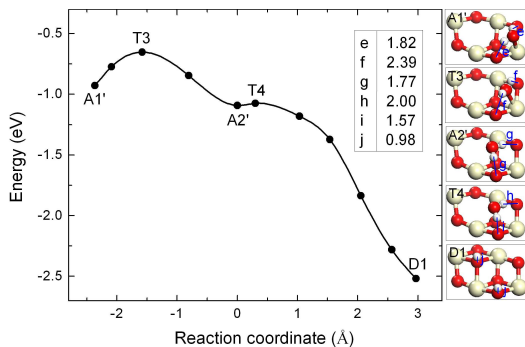


FIG. 6: (Color online) Variation in energy for the diffusion and dissociation of  $\text{H}_2\text{O}$  molecule on the reduced ceria(111) surface.

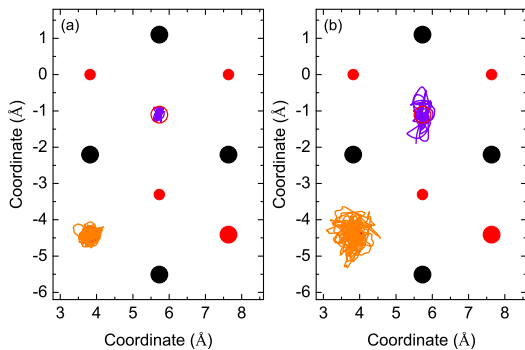


FIG. 7: (Color online) Projection on the reduced ceria(111) surface of the position of the oxygen atom corresponding to the OH species (purple) and the hydrogen atom (orange) from AIMD simulation at the temperature of 100 K (a) and 600 K (b), respectively. The red open circle denotes the oxygen vacancy position.

cess, which can be seen from the transition state T3 that has an O-down structure.

To determine the final configurations of the dissociation, we performed AIMD simulations for water on the reduced ceria(111) surface, starting from the adsorbed molecular site A2', at different temperatures (see Fig. 7). What is interesting, even at temperature as low as 100 K, is that the water monomer first oscillates around its equilibrium position and soon starts to dissociate into H and OH species almost *in situ*. It is found that the O atom of the OH species occupies the position of oxygen vacancy, with the O–H bond almost perpendicular to the surface, oscillating together with the surface. Whereas, another oscillating H atom of the dissociated water molecule is bonded to the adjacent top-layer O atom. Namely, hydroxyl surface forms upon the dissociation of water on the reduced ceria surface. This is the same at higher temperature of 600 K, only with a more intensive oscillation.

With this final dissociation configuration, now we return to the static CI-NEB calculations. As presented in

Fig. 6, the adsorption energy of the dissociated water state D1 was calculated to be  $-2.52$  eV, with the bond length between H and O of  $0.98$  Å. To reach the state D1, the system only needs to overcome a small barrier,  $0.02$  eV, corresponding to the low temperature 100K, as depicted in the AIMD simulations. At the transition state T4 leading to the dissociation, the interatomic distance between the O atom of the OH species and another H atom is quite small,  $1.12$  Å. These results consist well with previous experimental observation<sup>12</sup> and theoretical calculation<sup>16</sup>, while differ from the calculation with plain DFT<sup>17</sup> that resulted in a high activation energy  $2.35$  eV for water dissociation.

Interestingly, by static calculations we have also identified a semi-stable adsorption configuration with the adsorption energy  $-0.89$  eV, in which the O atom of the water occupies the position of the oxygen vacancy, with a no-H-bond configuration formed. This structure has once been considered as the most stable one on the reduced ceria surface<sup>16,17</sup>, and also a specious initial state for evolving hydrogen gas<sup>14</sup> at high coverage ( $0.5$ – $1.0$  ML). However, we find that the process of  $\text{H}_2$  molecule production is energetically unfavorable when compared with the formation of hydroxyl surface (about  $0.52$  eV higher in energy), therefore it cannot be observed in the AIMD simulations. Furthermore, it has been pointed out that the energy needed for  $\text{H}_2$  production is as high as  $2.05$  eV<sup>16</sup>, consistent with our results and the experimental observation that the reduced ceria(111) surface is resistant to being oxidized by water<sup>13</sup>.

#### IV. CONCLUSIONS

In conclusion, we have systematically studied the adsorption and dissociation behaviors of  $\text{H}_2\text{O}$  monomer on ceria(111) surface by first-principles calculations complemented with AIMD simulations. The most stable adsorption configurations on both the stoichiometric and reduced surfaces were identified, with the electronic structures analyzed in detail. Blocked by a diffusion barrier of  $0.51$  eV, water on the stoichiometric surface is very immobile up to at room temperature, while at higher temperature of 600 K, the water molecule can freely diffuse on the surface. For the reduced surface, We have found that the reaction of water and ceria is enhanced by the on-surface oxygen vacancy. It is facilitated for water to dissociate into H and OH species, only hindered by a small barrier of  $0.02$  eV, which was confirmed by the molecular dynamics simulations at temperature as low as 100 K. Besides, the reduced ceria(111) surface is resistant to being oxidized by water, in good accordance with the existing experimental results. The present results obtained at low water coverage afford to settle existing discrepancies about the behaviors of water on ceria surface, and provide a guiding line for deeply understanding the water-ceria surface interactions.

## Acknowledgments

This work was supported by NSFC under Grants No. 51071032 and No. 60821061.

- 
- \* Corresponding author; zhang\_ping@iapcm.ac.cn
- <sup>1</sup> A. Trovarelli, *Catal. Rev. - Sci. Eng.* 38, (1996) 439.
  - <sup>2</sup> Q. Fu, H. Saltsburg, M. Flytzani-Stephanopoulos, *Science* 301, (2003) 935.
  - <sup>3</sup> A. Siokou, R.M. Nix, *J. Phys. Chem. B* 103, (1999) 6984.
  - <sup>4</sup> N.V. Skorodumova, M. Baudin, K. Hermansson, *Phys. Rev. B* 69, (2004) 075401.
  - <sup>5</sup> Z. Yang, T.K. Wooa, M. Baudin, K. Hermanssona, *J. Chem. Phys.* 120, (2004) 7741.
  - <sup>6</sup> Y. Jiang, J.B. Adams, M. van Schilfgaarde, *J. Chem. Phys.* 123, (2005) 064701.
  - <sup>7</sup> M. Fronzi, A. Soon, B. Delley, E. Traversa, C. Stampfl, *J. Chem. Phys.* 131, (2009) 104701.
  - <sup>8</sup> F. Esch, S. Fabris, L. Zhou, T. Montini, C. Africh, P. Fornasiero, G. Comelli, R. Rosei, *Science* 309, (2005) 752.
  - <sup>9</sup> S. Torbrügge, M. Reichling, A. Ishiyama, S. Morita, O. Custance, *Phys. Rev. Lett.* 99, (2007) 056101.
  - <sup>10</sup> K. Otsuka, M. Hatano, A. Morikawa, *J. Catal.* 79, (1983) 493.
  - <sup>11</sup> C. Padeste, N.W. Cant, D.L. Trimm, *Catal. Lett.* 18, (1993) 305.
  - <sup>12</sup> L. Kundakovic, D. Mullins, S. Overbury, *Surf. Sci.* 457, (2000) 51.
  - <sup>13</sup> M.A. Henderson, C.L. Perkins, M.H. Engelhard, S. Thevuthasan, C.H.F. Peden, *Surf. Sci.* 526, (2003) 1.
  - <sup>14</sup> S. Kumar, P.K. Schellinga, *J. Chem. Phys.* 125, (2006) 204704.
  - <sup>15</sup> H. Chen, Y. Choi, M. Liu, M.C. Lin, *ChemPhysChem*, 8, (2007) 849.
  - <sup>16</sup> Z. Yang, Q. Wang, S. Wei, D. Ma, Q. Sun, *J. Phys. Chem. C* 114, (2010) 14891.
  - <sup>17</sup> M. Fronzi, S. Piccinin, B. Delley, E. Traversab, C. Stampfl, *Phys. Chem. Chem. Phys.* 11, (2009) 9188.
  - <sup>18</sup> V.I. Anisimov, F. Aryasetiawanz, A.I. Lichtenstein, *J. Phys.: Condens. Matter* 9, (1997) 767.
  - <sup>19</sup> S. Fabris, S. de Gironcoli, S. Baroni, G. Vicario, G. Balducci, *Phys. Rev. B* 71, (2005) 041102(R).
  - <sup>20</sup> D.A. Andersson, S.I. Simak, B. Johansson, I.A. Abrikosov, N.V. Skorodumova, *Phys. Rev. B* 75, (2007) 035109.
  - <sup>21</sup> C. Loschen, J. Carrasco, K.M. Neyman, F. Illas, *Phys. Rev. B* 75, (2007) 035115.
  - <sup>22</sup> J. Carrasco, F. Illas, N. Lopez, *Phys. Rev. Lett.* 100, (2008) 016101.
  - <sup>23</sup> G. Kresse, J. Furthmuller, *Phys. Rev. B* 54, (1996) 11169.
  - <sup>24</sup> J.P. Perdew, K. Burke, M. Ernzerhof, *Phys. Rev. Lett.* 77, (1996) 3865.
  - <sup>25</sup> S.L. Dudarev, G.A. Botton, S.Y. Savrasov, C.J. Humphreys, A.P. Sutton, *Phys. Rev. B* 57, (1998) 1505.
  - <sup>26</sup> H.J. Monkhorst, J.D. Pack, *Phys. Rev. B* 13, (1976) 5188.
  - <sup>27</sup> G. Henkelman, B.P. Uberuaga, H. Jónsson, *J. Chem. Phys.* 113, (2000) 9901.
  - <sup>28</sup> H. Jónsson, G. Mills, K.W. Jacobsen, in *Classical and Quantum Dynamics in Condensed Phase Simulations*, edited by B.J. Berne et al. World Scientific, Singapore, 1998.
  - <sup>29</sup> S. Nosé, *J. Chem. Phys.* 81, (1984) 511; S. Nosé, *Prog. Theor. Phys. Suppl.* 103, (1991) 1.
  - <sup>30</sup> S.J. Duclos, Y.K. Vohra, A.L. Ruoff, A. Jayaraman, G.P. Espinosa, *Phys. Rev. B* 38, (1988) 7755.
  - <sup>31</sup> L. Gerward, J.S. Olsen, *Powder Diffr.* 8, (1993) 127.
  - <sup>32</sup> L. Gerward, J.S. Olsen, L. Petit, G. Vaitheeswaran, V. Kanchana, A. Svane, *J. Alloys Compd.* 400, (2005) 56.
  - <sup>33</sup> A. Nakajima, A. Yoshihara, M. Ishigame, *Phys. Rev. B* 50, (1994) 13297.
  - <sup>34</sup> F. Birch, *Phys. Rev.* 71, (1947) 809.
  - <sup>35</sup> E. Wuilloud, B. Delley, W.-D. Schneider, Y. Baer, *Phys. Rev. Lett.* 53, (1984) 202.
  - <sup>36</sup> D. Eisenberg, W. Kauzmann, *The Structure and Properties of Water*, Oxford University Press, New York, 1969.
  - <sup>37</sup> N.V. Skorodumova, S.I. Simak, B.I. Lundqvist, I.A. Abrikosov, B. Johansson, *Phys. Rev. Lett.* 89, (2002) 166601.